JOURNAL OF GEOPHYSICAL RESEARCH, VOL. 101, NO. B8, PAGES 17,795–17,811, AUGUST 10, 1996

Stability of a frictional, cohesive layer on a viscous substratum: Variational formulation and asymptotic solution

Y. M. Leroy

Laboratoire de Mécanique des Solides, CNRS URA 317, Ecole Polytechnique, Palaiseau, France

N. Triantafyllidis

Department of Aerospace Engineering, University of Michigan, Ann Arbor

Abstract. This contribution is concerned with the stability of a frictional, cohesive material layer, called the overburden, resting on a viscous, incompressible layer of lower density referred to as the substratum. The viscous layer is either perfectly bonded or free to slip with no friction on a rigid basement. The in situ stress is assigned a realistic gradient in the overburden and is assumed to be purely hydrostatic in the substratum. A general variational formulation of the linearized stability problem for the stratified system is obtained in which the viscous response of the substratum provides the characteristic time. To a given state of stress and perturbation corresponds a rate of growth or decay which is calculated by an asymptotic method for small overburden thickness compared to the perturbation wavelength. It is found that the substratum's thickness influences the rate of growth of the instability if its product by the perturbation wavenumber is smaller than 3 or 4, depending on the type of boundary condition at the basement. However, these conditions and the substratum thickness have no influence on neutral stability. Furthermore, the conditions for stability depend on the tectonic stress distribution in the overburden and not solely on the density contrast, as is the case for viscoelastic systems. It is also shown that the classical flow theory of plasticity adopted for the overburden, which successfully captures the onset of folding, fails to predict initiation of faulting for similar stress conditions.

Introduction

A variety of geological problems, such as the folding of oceanic lithospheres, the development of sedimentary basins and the formation of salt domes, leads to question the stability of a competent layer resting over a viscous substratum of lower density and a rigid basement. The elastoplasticity model we propose for the overburden permits us to assess the competing influence of the tectonic forces and their gradients with depth, the density contrast, and the overburden stiffness (a nonlinear function of stress) on the stability of the stratified system. Furthermore, since the overburden is modeled as a frictional, cohesive material, it is then possible to study simultaneously two classes of instabilities: diffuse modes (such as folding) and localized mode (faulting).

The geometry of the model just described is common to many studies of folding, including the work of *Smoluchowski* [1909] on the stability of an elastic plate on a fluid substratum. This elastic plate solution, as given by *Ramberg and Stephansson* [1964], was essential for developing an understanding of the mechanics of folding of stratified media affected by gravity. To improve on the elastic plate model, *Biot* [1961], *Ramberg and Stephansson* [1964], and *Biot and Odé* [1965] accounted for the rate sensitivity of crustal rocks by using linear, viscoelastic constitutive models.

For layers with a pronounced contrast in viscosity, laboratory experiments by *Biot et al.* [1961] showed the validity of linear stability analysis of equilibrium states for which any time evolution of the fundamental solution (e.g., uniform rate of shortening) is disregarded. However, these theoretical predictions, which relate instability wavelength and viscosity ratio, were not sufficient to explain the field observations by *Sherwin and Chapple* [1968] of hundreds of isolated folds with a low contrast in viscosity. The discrepancy between theory and observation was partly alleviated by the same authors who showed the influence on the wavelength selection of the rate of nominal compression. Another improvement of the plate model came with the introduction of more complex rheology. The need for a nonlinear constitutive behavior had indeed long been recognized [*Biot,* 1961] and was discussed by various

Paper number 96JB01340.
0148-0227/96/96JB-01340$09.00

authors. For example, *Chapple* [1969] introduced the two models of linear viscosity and perfect plasticity for low and high stress levels, respectively, in modeling the initiation of a plastic hinge at the crest of a finite amplitude fold. However, it was only in the mid 1970s that the results of a linear stability analysis, which included a power law fluid rheology and accounted for the evolution of the fundamental solution, were first published [*Fletcher,* 1974].

Viscoelastic models differing in complexity have been applied successfully to predict folding on length scales ranging from centimeter scales [*Sherwin and Chapple,* 1968] to that of lithospheric thickness [*McAdoo and Sandwell,* 1985; *Martinod and Davy,* 1992]. Often, secondary features associated with folding such as cracks and distributed faulting have been disregarded in these studies. This simplification was based on the assumption that deformation beyond the elastic limit is ductile and diffuse on the length scale chosen for the structural stability analysis. This hypothesis was explicitly adopted by *Fletcher and Hallet* [1983] for their study of the unstable extension of the lithosphere. They, however, considered a power law fluid with a large exponent in an attempt to mimic the distributed faulting they disregarded in the brittle surface layer. Such an approach is not sufficient if both diffuse instability modes, such as folding or necking, and localized modes in the form of faults are of interest. Indeed, non-Newtonian fluid models used so far in structural stability predictions do not include any of the appropriate features, such as grain size reduction or geometrical softening in crystalline materials, which are conducive to strain localization [*Poirier,* 1980]. The absence of a mechanism to nucleate faults has been palliated by introducing directly and in a discrete manner a single or a few faults which could accommodate displacement discontinuities in a structural problem [*van Wees and Cloetingh,* 1994; *Wallace and Melosh,* 1994]. This paper goes one step further and recognizes that pervasive fracturing results in continuous inelastic deformation. Indeed, it is assumed that the observer at the macroscale is unable to single out a fault justifying the application of a plasticity model for continua.

Laboratory tests on crustal rocks at confining pressures corresponding to a depth of several kilometers show that the strength of specimens increases with the accumulation of permanent deformation by several tens of a percent until a maximum load is reached [*Griggs and Handin,* 1960]. Such a behavior can be modeled with an elastoplasticity law [e.g., *Rudnicki and Rice,* 1975]. The inelasticity before failure described above, which cannot be accounted for with steady state creep laws, has been related to the initiation and the coalescence of micro-cracks (for quartzite specimens [e.g., *Hallbauer et al.* 1973]). Analogue materials used in scaled geophysical models often have a similar behavior. This is the case of the composite material designed by *Shemenda* [1992] for his models of the lithosphere which develop both folding and faulting under compressive loading. Indeed, Shemenda's material requires approximately 10 percent deformation before the maximum strength is reached in a shear test. Sand, which is often employed as an analogue material, has similar properties as it can be judged from the experimental work of *Tatsuoka et al.* [1993] for a quartz-rich, poorly graded, and fine sand tested in plane-strain compression under a confining pressure equivalent to a few meters of lithostatic pressure.

Time-independent elastoplasticity models have been applied successfully to determine the conditions for initiation of faulting. *Odé* [1960] shows that slip-line theory developed for rigid-plastic materials explains and can be used to analyze faulting under plane-strain conditions. *Rudnicki and Rice* [1975] and *Rice* [1976] show the sensitivity of fault initiation to the details of the hardening response of the material beyond first yield and to the exact deformation mechanism activated. *Mandl* [1988] has eloquently advocated for many years the use of elastoplasticity theories for modeling tectonic faults in structural geology.

It thus appears that the constitutive models traditionally used in structural stability or buckling analyses (elastic, viscoelastic), differ from models considered to predict initiation of faulting (elastoplastic). Indeed, only a few papers on geological stability problems deal with elastoplastic constitutive models. *Dorris and Nemat Nasser* [1980] considered the stability problem of a finite thickness layer composed of a Von Mises material and resting on an elastic half-space, disregarding the in situ stress gradients. *Triantafyllidis and Lehner* [1993] considered the interfacial instability between a solid and a fluid half-space, accounting for in situ stress gradients. *Triantafyllidis and Leroy* [1994] extended this analysis by considering a finite thickness overburden composed of a frictional material. The present study builds on the previous work by the same authors in allowing for a buoyant substratum of finite thickness and exploring the unstable regime rather than the neutral stability conditions alone. Frictional material properties are represented by nonassociated plasticity models, the introduction of which results in a nonsymmetric stability operator. The reader interested in theoretical aspects of solving this class of nonsymmetric stability problems is referred to *Triantafyllidis and Leroy* [1994] for further discussion.

There are three research directions which could benefit from the results of a structural stability analysis with frictional material models. First, there is a need to predict the distribution and evolution of stress and the onset of faulting in stratified, folded systems. This paper provides some insight on the potential sensitivity of such predictions to the details of the constitutive model chosen. It points to the necessity in the future to construct a plasticity model starting from a description of pervasive fracturing. An attempt in that direction for the study of a fractured reservoir in an anticline can be found in the work of *Leroy and Sassi* [1996]. The link between pervasive fracturing and the construction of bulk deformation is then seen as the means to predict the permeability of fractured formation. The second

research direction is in the mechanics of diapirs. The emplacement of diapirs has usually been modeled as an instability in viscoelastic layered systems with a density contrast [*Biot and Odé,* 1965], disregarding the potential piercement mechanism which may operate in a cohesive overburden. The role of cohesive competent layers in the formation of domes has been established with analogue models [*Nettleton and Elkins,* 1947; *Parker and McDowell,* 1955] and was analyzed theoretically for an overburden modeled as a rigid, perfectly plastic material [*Bishop,* 1978]. In that instance, limit loads have been proposed to constrain the conditions for the onset of piercement [*Charo and Habib,* 1987]. The approach considered here combines the advantages of the two theoretical models discussed above: the geometric effects present in the viscoelastic approach, which are essential for stability predictions, are included, and the overburden cohesion, considered in the classical perfect-plasticity theory, is also accounted for. Our results, once completed by nonlinear numerical simulations, could thus be used to determine the regimes, defined by the model geometry, tectonic stress, density contrast and overburden cohesion, for which the structural instability dominates and for which the piercement in a passive overburden is the driving force for diapirism. Third, recent advances in scaled laboratory experiments and the possibility of fine characterization of analogue materials should permit the comparison of experimental and theoretical predictions on the onset of instability modes such as folding and faulting. Such a comparison is proposed in the sequel of this work in which the stability predictions for a prototype of a section through the Campos salient, offshore Brazil [*Demercian et al.,* 1993] are compared with those obtained for a scaled version of a prototype designed for laboratory testing. In particular, the first stage of folding during the Albian is well captured with our analysis which provides an estimate of the tectonic stress for onset of folding. This stress is quantitatively comparable to the one inferred with the hypothesis that gravitational gliding of sediments is the source of the compressional tectonic force. A similar stability analysis with the scaled prototype shows the difficulty in capturing folding for the appropriate stress level with granular material such as quartz grain sand.

The contents of this paper are as follows. In the second section the general elastoplasticity model adopted is first presented, the conditions for the onset of faulting are then discussed, and finally the appropriate variational formulation of the stability problem is proposed. Note that the strain rate sensitivity of the overburden is disregarded since the rate-controlling mechanism is attributed to the deformation of the viscous layer. A redistribution condition at the top surface which models erosion [*Biot and Odé,* 1965] is also adopted. For deriving the variational statement, the influence of the viscous substratum is characterized by two sets of influence functions corresponding to either a perfect bond or a frictionless slip condition with respect to the rigid basement. The details of the derivation of these functions is summarized in the first part of the supplement to this paper[1]. The condition of frictionless slip could be explained by the presence of a thin layer of low viscosity at the interface with the basement. This resembles, for example, the bishofite salt layer found in the Northern German Zechstein basin [*Coelewij et al.,* 1978] or similar highly ductile layers elsewhere. The perfect bond and frictionless slip are two extreme cases which could be related by a varying friction coefficient, as was considered by *Smith* [1975] for two viscous layers. The third section is devoted to the asymptotic solution of the stability variational form for an overburden which is thin compared to the instability wavelength. The complete solution is presented in the appendix and the details of the derivation are found in the second part of this paper's supplement. This plate-type solution accounts for the stress gradient present in the overburden and is valid for a general class of elastoplasticity models. It is applied to the flow theory version of *Rudnicki and Rice's* [1975] model in the fourth section. This section also contains a parametric analysis for the influence on stability of the in situ stress distribution and work-hardening properties of the overburden material. The lack of sensitivity to the work-hardening properties together with the absence of any detection of faulting illustrates the limitations of the flow theory version of the Rudnicki and Rice model for the class of problems of interest here. A summary of these results and a discussion on the role of the plasticity model for the onset of faulting and folding are provided in the last section.

Model Formulation

The derivation of the variational formulation of the structural stability problem is the prime objective of this section. As a preliminary step, we discuss the in situ stress description adopted, the constitutive response of the solid and viscous materials and the condition of strong ellipticity. The violation of that condition signals potential discontinuities in the velocity gradient which are interpreted as the onset of faulting in the overburden. It is only in the absence of faulting, thus in the elliptic regime of the governing differential equations, that the predictions of the structural stability analysis are valid.

In Situ Stress, Material Law, and Onset of Faulting

The reference configuration, presented in Figure 1a, consists of an overburden of thickness H_a and density $\overset{a}{\rho}$ resting on a substratum of thickness H_b and density $\overset{b}{\rho}$. A set of coordinate axes (x_1, x_2, x_3) is introduced with the x_1 axis lying on the planar interface between

Supporting appendix is available on diskette or via Anonymous FTP from kosmos.agu.org, directory APEND (Username = anonymous, Password = guest). Diskette may be ordered from American Geophysical Union, 2000 Florida Avenue, N.W., Washington, DC 20009 or by phone at 800-966-2481; $15.00. Payment must accompany order.

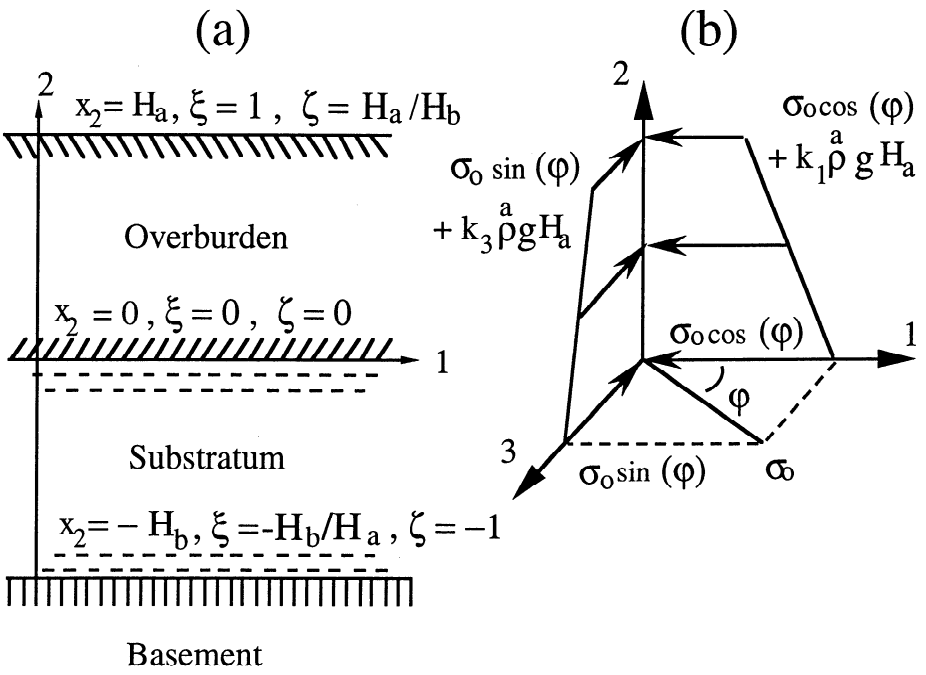

Figure 1. Geometry of the model problem and in situ stress distribution in the overburden. A layer of frictional, cohesive material, the overburden, rests on a layer of viscous fluid. The two strata lie on a rigid basement, as shown in the cross section in Figure 1a. The overburden sustains its own weight and a tectonic stress distribution which is illustrated in Figure 1b.

the frictional overburden and the viscous substratum and with gravity acting along the $-x_2$ direction. Normalized coordinates $\xi \equiv x_2/H_a$ and $\zeta \equiv x_2/H_b$ are introduced for convenience. Quantities associated with the top layer are marked by the letter a (a for above) in superscript or in subscript. Similarly, the letter b (b for below) designates quantities attached to the substratum.

The first preliminary step in formulating this stability problem is the description of the initial stress state. The principal in situ stress direction (Andersonian) in the overburden coincides with the orientation of the coordinate system adopted. It is illustrated in Figure 1b and takes the form

$$\begin{aligned} \overset{a}{\sigma}_{11}(\xi) &= \sigma_0 \cos(\varphi) + k_1 \overset{a}{\rho}\, g H_a \xi\,, \\ \overset{a}{\sigma}_{22}(\xi) &= \overset{a}{\rho}\, g H_a (\xi - 1)\,, \\ \overset{a}{\sigma}_{33}(\xi) &= \sigma_0 \sin(\varphi) + k_3 \overset{a}{\rho}\, g H_a \xi\,. \end{aligned} \tag{1}$$

The value of the principal stresses at the interface between the overburden and substratum is parameterized by the scalar σ_0 and the angle φ. The variation of φ from 0 to $\pi/2$ results in a change in $\overset{a}{\sigma}_{11}(0)$ and $\overset{a}{\sigma}_{33}(0)$ from σ_0 to 0 and from 0 to σ_0, respectively. The vertical stress corresponds to the lithostatic pressure. The two parameters k_1 and k_3 provide information on the gradient with depth of $\overset{a}{\sigma}_{11}$ and $\overset{a}{\sigma}_{33}$, respectively. The values of these stress gradient parameters are typically of order 1 in sedimentary basins [*Breckels and van Eekelen,* 1982] and could be as high as 2 in regions where thrust faulting and folding are the predominant mode of deformation [*McGarr and Gay,* 1978]. The stress state in the substratum is hydrostatic with a gradient controlled by the increase in the lithostatic pressure:

$$\overset{b}{\sigma}_{11}(\zeta) = \overset{b}{\sigma}_{22}(\zeta) = \overset{b}{\sigma}_{33}(\zeta) = -\overset{a}{\rho}\, g H_a + \overset{b}{\rho}\, g \zeta H_b\,. \tag{2}$$

Pore pressure has been disregarded in this analysis although it could have been accounted for within the proposed theoretical framework. It is preferred, for sake of simplicity, to postpone the investigation of its role in structural stability. For the present analysis, it suffices for justifying our choice to claim that Terzaghi effective stress principle applies, despite the nonlinear range of deformation, and that the system considered is fully drained on the geological timescale of interest.

The second preliminary step is a brief discussion of the time-independent elastoplasticity model considered for the overburden. The description (1) adopted for the stress state permits us to estimate, at any point in the overburden, the current yield stress and the internal variables of the plasticity model [e.g., *Martin,* 1975] if a loading path in stress space is postulated. For simplicity, a proportional loading path is assumed. The evaluation of the internal variables is now illustrated by means of a simple plasticity model with a pressure-sensitive yield surface and a single internal variable, the accumulated plastic strain γ^p. From the stress state (1), one determines the stress invariants or related quantities such as the equivalent shear stress τ and pressure p. The yield criterion defined by $\phi(\tau, p) - f(\gamma^p) \leq 0$ is respected for all stress states (1), a condition from which the value of the internal variable γ^p is extracted

as follows. It is first assumed that laboratory tests have provided us with the work hardening function $f(\gamma^p)$ and it is postulated that the current stress state has been reached by proportional loading such that $\phi(\tau, p)$ is equal to the measured $f(\gamma^p)$, if plasticity has occurred. Such a condition provides directly the value of the internal variable γ^p. Knowledge of the stress and internal variables distribution in the overburden permit us to specify the incremental response of each material point. That incremental response could be elastic or elastoplastic depending on the orientation of the stress increment with respect to the elastic region in stress space. For this linear stability analysis, it is further assumed that permanent deformation will result from any stress perturbation if plastic deformation was necessary to accommodate the in situ stress. Possible elastic unloading are thus disregarded. This assumption is equivalent to the choice of a comparison solid proposed by *Hill* [1958] for bifurcation analysis. The validity of this assumption is explored by numerical means by *Massin et al.* [1996].

Each material point is identified by its coordinates X_i and x_i in the reference and the current configuration, respectively. The difference between these two positions, $x_i - X_i$, defines the components of the displacement field u_i. The rate of displacement is $\dot{u}_i$ and the displacement gradient is $u_{i,j}$. The time derivative is denoted by a superimposed dot and a comma followed by an index stands for partial differentiation with respect to the corresponding direction. The relevant form of the constitutive response for each layer relates the rate of the first Piola-Kirchhoff stress Π_{ij} to the first and second rates of the displacement gradient $\dot{u}_{i,j}$ and $\ddot{u}_{i,j}$:

$$\begin{aligned} \dot{\Pi}_{ji} &= \overset{a}{L}_{ijkl}\,\dot{u}_{l,k} \qquad 0 \le x_2 \le H_a\,, \\ \dot{\Pi}_{ji} &= \overset{b}{L}_{ijkl}\,\dot{u}_{l,k} + \overset{b}{M}_{ijkl}\,\ddot{u}_{l,k} \qquad -H_b \le x_2 \le 0\,. \end{aligned} \tag{3}$$

The definition of the stress tensor introduced above and its relation to the Cauchy stress, used to describe the in situ stress (1), can be found in continuum mechanics textbooks [e.g., *Ogden,* 1984]. General expressions for the moduli $\overset{a}{L}_{ijkl}$ and the definition of the objective rate chosen to define the incremental response are given by *Triantafyllidis and Leroy* [1994]. The reader could also find further information on the incremental response of solids under initial stress in the book by *Biot* [1965] and in *Hill and Hutchinson* [1975]. Note that the main difference in (3) between the overburden and the substratum is the absence of instantaneous viscosities $\overset{b}{M}_{ijkl}$ in the top layer where the response is assumed to be time independent.

The present stability analysis is restricted to sufficiently smooth, structural modes such as buckling (folding). It is valid only if local instabilities in the form of shear bands (faulting) is precluded. Consequently, the stability calculations will only apply if the strong ellipticity condition is satisfied at every point in the overburden:

$$\overset{a}{L}_{ijkl}(\xi) m_i n_j n_k m_l > 0 \quad 0 \le \xi \le 1\,, \tag{4}$$

for every set of unit vectors $\mathbf{m}$ and $\mathbf{n}$. Repeated indices in (4) and in what follows imply summation from 1 to 3. If (4) does not hold at a point ξ, then a discontinuity in the velocity gradient must be present. This discontinuity, which initiates when (4) is an equality, is along a line of normal $\mathbf{n}$ passing through ξ. If the vector $\mathbf{m}$ is perpendicular to the normal direction, the discontinuity is of a fault type. In what follows, we make use of equation 29 of *Triantafyllidis and Leroy* [1994], which is equivalent to (4), to check for the condition of strong ellipticity.

Formulation of the Stability Problem

The starting point for the derivation of the variational formulation of the stability problem is the rate form of the equilibrium equations. A linear perturbation analysis is then conducted followed by a Fourier transform which takes advantage of the independence of the equilibrium state with respect to the x_1 coordinate. This leads to a variational form in which the role of the substratum is replaced by a set of influence functions. An inspection of these functions permits us to draw some first conclusions on the role of the substratum thickness and to compare those with *Ramberg's* [1960, 1961] results. Some of the steps to be followed to set up the stability formulation are similar to those considered by *Triantafyllidis and Leroy* [1994]. We shall make reference to this work for sake of conciseness and will concentrate on new features of the present analysis.

An updated Lagrangian formulation is adopted for which the reference configuration is identified with the current one (i.e., $u_i = 0$, but $\dot{u}_i, \ddot{u}_i \neq 0$). The rate form of the equilibrium equations and the interface and boundary conditions are written as

$$\dot{\Pi}_{ij,i} = 0 \quad -H_b \le x_2 \le H_a\,, \tag{5}$$

$$[\![\dot{\Pi}_{2j}]\!] = 0\,,\ [\![\dot{u}_j]\!] = 0 \quad x_2 = 0\,, \tag{6}$$

$$\dot{\Pi}_{21} = 0\,, \dot{u}_1 = 0, \text{ or } \dot{u}_1 = \dot{u}_2 = 0 \quad x_2 = -H_b\,, \tag{7}$$

$$\dot{\Pi}_{2j} = s\,\overset{a}{\rho}\, g \dot{u}_2 \delta_{j2} \quad x_2 = H_a\,, \tag{8}$$

in which δ_{j2} is the Kronecher delta (equal to 1 if j is set to 2 and to 0 otherwise). The notation $[\![f(x)]\!]$ stands for the jump in the generic function f across the position x: $f(x^+) - f(x^-)$. The incremental equilibrium equation (5) is satisfied at any point in the stratified system. Equations (6) dictate the continuity of traction and displacement rates across the overburden-substratum interface. Equations (7) express the two types of boundary conditions at the bottom of the substratum: the frictionless contact case, characterized by no shear stress and no vertical separation between substratum and basement and the perfect bonding case, for which no point in the viscous substratum in contact with the basement can be displaced. The last equation (8), which applies at the free surface of the overburden, follows from a proposition of *Biot and Odé* [1965] to model erosion. For a zero value of the scalar s, there

is a traction-free boundary condition with no erosion. If the same scalar is set to 1, erosion or more precisely redistribution takes place: upheaved sections of the top surface are eroded away and redeposited in the regions which have subsided. This redistribution condition is translated into a mixed boundary condition between traction and displacement rates by prescribing the normal component of the traction to equal the lithostatic pressure of the missing or extra material. No characteristic time is introduced for this process which is assumed to be short compared to the relaxation of the perturbed system.

Before embarking on the linear perturbation of the governing equations (3) and (5-8), we adopt for simplicity the assumption of plane-strain deformation although a fully three-dimensional setting of the problem has been proposed so far. The stability problem is thus restricted to the (x_1, x_2) plane and its solution is independent of the x_3 coordinate. The system sustaining the state of prestress (1) is subjected to a perturbation: all field quantities are written as a sum of a fundamental value, marked by the superscript 0, and a time-dependent perturbation with amplitude ε, small compared to 1. The stress and displacement fields of the perturbed system are thus assumed to be

$$\begin{aligned}\Pi_{ij}(x_1,x_2,t) &= \overset{0}{\Pi}_{ij}(x_1,x_2) \\ &\quad + \varepsilon \exp(\lambda t)\widehat{\Pi}_{ij}(x_1,x_2) + \mathcal{O}(\varepsilon^2)\,, \\ u_i(x_1,x_2,t) &= \overset{0}{u}_i(x_1,x_2) \\ &\quad + \varepsilon \exp(\lambda t)\widehat{u}_i(x_1,x_2) + \mathcal{O}(\varepsilon^2)\,, \end{aligned} \tag{9}$$

in which $\widehat{\Pi}_{ij}$ and $\widehat{u}_i$ are the mode of perturbation in stress and displacement. Note that any term smaller than those of first-order are disregarded in this linear stability analysis. The fundamental solution is considered to be an equilibrium state and, consequently, time and spatial dependence of the perturbation has been separated in (9) and an exponential function introduced for the evolution with time. The stability exponent λ is in general a complex number and its real part determines the stability of the system. A positive real part signals an unstable equilibrium state. Conversely, if all solutions of the stability problem require the real part of the parameter λ to be negative, the system is said to be stable. The superscript 0, denoting the fundamental values of the field quantities, is omitted in what follows, since all moduli and stresses in the formulation of the stability problem are evaluated at the reference state, which is time independent.

Substitution of expressions (9) for the field perturbations into the constitutive equations (3) and incremental equilibrium equations (5), leads to a system of equations equivalent to equation 5 of *Triantafyllidis and Leroy* [1994]. This equation has to be supplemented with the new boundary conditions at the basement:

$$\begin{aligned}&(\overset{b}{L}_{12kl} + \lambda\, \overset{b}{M}_{12kl})\,\widehat{u}_{l,k} = 0\,,\ \widehat{u}_2 = 0 \\ &\qquad \text{or} \quad \widehat{u}_1 = \widehat{u}_2 = 0\,, \quad x_2 = -H_b\ , \end{aligned} \tag{10}$$

in which λ and $\widehat{u}_i$ have the same definition as in (9).

The analysis is greatly simplified by the condition of material orthotropy with respect to the coordinate system. This orthotropy condition, found in many studies on bifurcation [*Biot,* 1965; *Hill and Hutchinson,* 1975], relies on the principal stress directions of the fundamental solution coinciding with the coordinate system directions and implies that the normal-to-shear components of the moduli L_{ijkl} and M_{ijkl} are zero (e.g., $L_{1211} = 0$). The reader is referred to *Triantafyllidis and Leroy* [1994] for further details. A second feature of the fundamental solution is that the coefficients in the governing linear ordinary differential equations are independent of the x_1 coordinate. The equilibrium equations can thus be simplified and the following Fourier transform: $U_1(\omega, x_2) = \mathcal{F}\big[\widehat{u}_1(x_1,x_2); x_1 \to \omega\big]$, $-iU_2(\omega,x_2) = \mathcal{F}\big[\widehat{u}_2(x_1,x_2); x_1 \to \omega\big]$ is adopted. The application of this Fourier transform to the equilibrium equations and boundary conditions leads to a system of two ordinary differential equations:

$$\begin{aligned}&-\omega^2 N_{1111}U_1 + \omega N_{1122}U_{2,2} + \omega(N_{1212}U_2)_{,2} \\ &\quad +(N_{1221}U_{1,2})_{,2} = 0 \quad -H_b \le x_2 \le H_a\,, \\ &-\omega^2 N_{2112}U_2 - \omega N_{2121}U_{1,2} - \omega(N_{2211}U_1)_{,2} \\ &\quad +(N_{2222}U_{2,2})_{,2} = 0 \quad -H_b \le x_2 \le H_a\,, \end{aligned} \tag{11}$$

with

$$\begin{aligned} N_{ijkl}(x_2,\lambda) &\equiv \overset{a}{L}_{ijkl}(x_2) \qquad 0 \le x_2 \le H_a\,, \\ N_{ijkl}(x_2,\lambda) &\equiv \overset{b}{L}_{ijkl}(x_2) + \lambda \overset{b}{M}_{ijkl}(x_2) \\ &\qquad -H_b \le x_2 \le 0; \end{aligned} \tag{12}$$

and complemented by the three sets of interface and boundary conditions:

$$\begin{aligned}[\![\omega N_{1212}U_2 + N_{1221}U_{1,2}]\!] &= 0\,, [\![U_1]\!] = 0 \\ [\![\omega N_{2211}U_1 - N_{2222}U_{2,2}]\!] &= 0\,, [\![U_2]\!] = 0\,; \end{aligned} \tag{13}$$

$$\begin{aligned}\omega N_{1212}U_2 + N_{1221}U_{1,2} = 0 \text{ or } \quad U_1 &= 0 \\ U_2 &= 0\,; \end{aligned} \tag{14}$$

$$\begin{aligned}\omega N_{1212}U_2 + N_{1221}U_{1,2} &= 0 \\ \omega N_{2211}U_1 - N_{2222}U_{2,2} &= -s\rho g U_2\,; \end{aligned} \tag{15}$$

which are applied at x_2 equal 0, $-H_b$ and H_a, respectively.

The variational form of the stability problem is obtained by multiplying the first and second differential equations in (11) by the arbitrary functions $\delta U_1(\xi)$ and $\delta U_2(\xi)$, respectively. Subsequent integration by parts over the overburden (from x_2 equal to 0 to H_a) and the account of the interface and boundary conditions results in

$$\int_0^1 \Big[\Big(\frac{\overset{a}{L}_{1221}}{\omega H_a}\frac{dU_1}{d\xi} + \overset{a}{L}_{1212}U_2\Big)\frac{1}{\omega H_a}\frac{d\delta U_1}{d\xi} + \Big(-\frac{\overset{a}{L}_{1122}}{\omega H_a}\frac{dU_2}{d\xi}$$

$$+\overset{a}{L}_{1111}U_1)\delta U_1+(\frac{\overset{a}{L}_{2222}}{\omega H_a}\frac{dU_2}{d\xi}-\overset{a}{L}_{2211}U_1)\frac{1}{\omega H_a}\frac{d\delta U_2}{d\xi}$$
$$+(\frac{\overset{a}{L}_{2121}}{\omega H_a}\frac{dU_1}{d\xi}+\overset{a}{L}_{2112}U_2)\delta U_2\Big]d\xi$$
$$-\frac{1}{(\omega H_a)^2}\Big[s\,\overset{a}{\rho}\,gHU_2\delta U_2\Big]_{\xi=1}+\frac{1}{\omega H_a}\Big[\Big((\overset{b}{L}_{1221}$$
$$+\lambda\overset{b}{M}_{1221})\frac{1}{\omega H_a}\frac{dU_1}{d\xi}+(\overset{b}{L}_{1212}+\lambda\overset{b}{M}_{1212})U_2\Big)\delta U_1$$
$$+\Big((\overset{b}{L}_{2222}+\lambda\overset{b}{M}_{2222})\frac{1}{\omega H_a}\frac{dU_2}{d\xi}$$
$$-(\overset{b}{L}_{2211}+\lambda\overset{b}{M}_{2211})U_1\Big)\delta U_2\Big]_{\xi=0^-}=0\,. \qquad (16)$$

The presence of ωH_a in the denominator of the various terms in (16) relies on the assumption that ω differs from zero. The particular case of a zero wavenumber can be studied directly from equations (1) to (10), but is of no consequence to the present analysis.

To simplify (16), it is desirable to eliminate the derivative of the eigenmode U_i evaluated on the substratum side of the interface. The expressions relating $dU_i/d\xi$ and U_i at the interface ($\xi = 0^-$) can be obtained analytically for the case of an incompressible substratum in terms of its dimensionless thickness ωH_b and its instantaneous shear viscosity $\overset{b}{\mu}$. The details of these derivations are deferred to the first part of the supplement to this paper. The final expression for the variational statement of stability reads

$$\int_0^1\Big[(\frac{\overset{a}{L}_{1221}}{\omega H_a}\frac{dU_1}{d\xi}+\overset{a}{L}_{1212}U_2)\frac{1}{\omega H_a}\frac{d\delta U_1}{d\xi}+(\frac{-\overset{a}{L}_{1122}}{\omega H_a}\frac{dU_2}{d\xi}$$
$$+\overset{a}{L}_{1111}U_1)\delta U_1+(\frac{\overset{a}{L}_{2222}}{\omega H_a}\frac{dU_2}{d\xi}-\overset{a}{L}_{2211}U_1)\frac{1}{\omega H_a}\frac{d\delta U_2}{d\xi}$$
$$+(\frac{\overset{a}{L}_{2121}}{\omega H_a}\frac{dU_1}{d\xi}+\overset{a}{L}_{2112}U_2)\delta U_2\Big]d\xi$$
$$-\frac{1}{(\omega H_a)^2}\Big[s\,\overset{a}{\rho}\,gH_aU_2\delta U_2\Big]_{\xi=1}+\frac{1}{\omega H_a}\Big[\overset{a}{\rho}\,gH_a(U_1\delta U_2$$
$$+U_2\delta U_1)+\frac{\overset{b}{\rho}\,gH_b}{\omega H_b}U_2\delta U_2\Big]_{\xi=0}+\frac{\Lambda}{\omega H_a}\Big[(f_{11}U_1$$
$$+f_{12}U_2)\delta U_1+(f_{21}U_1+f_{22}U_2)\delta U_2\Big]_{\xi=0}=0\,. \qquad (17)$$

Equation (17) constitutes a generalized eigenvalue problem for the stability exponent Λ (defined as $2\lambda\overset{b}{\mu}$). The functions f_{ij} of the substratum's dimensionless thickness ωH_b are for a perfect bond

$$f_{11}\equiv\frac{\cosh(\omega H_b)\sinh(\omega H_b)-\omega H_b}{\sinh^2(\omega H_b)-(\omega H_b)^2}\,,$$
$$f_{12}\equiv\frac{-(\omega H_b)^2}{\sinh^2(\omega H_b)-(\omega H_b)^2}\equiv f_{21}\,,$$
$$f_{22}\equiv\frac{\cosh(\omega H_b)\sinh(\omega H_b)+\omega H_b}{\sinh^2(\omega H_b)-(\omega H_b)^2}\,; \qquad (18)$$

and for a frictionless contact at the substratum-basement interface

$$f_{11}\equiv\frac{\sinh^2(\omega H_b)}{\cosh(\omega H_b)\sinh(\omega H_b)-\omega H_b}\,,$$
$$f_{12}\equiv\frac{-\omega H_b}{\cosh(\omega H_b)\sinh(\omega H_b)-\omega H_b}\equiv f_{21}\,,$$
$$f_{22}\equiv\frac{\cosh^2(\omega H_b)}{\cosh(\omega H_b)\sinh(\omega H_b)-\omega H_b}\,, \qquad (19)$$

respectively. Note that the influence of the substratum is only felt through these functions. Consequently, the conditions of neutral stability ($\Lambda = 0$) are affected neither by the geometry of the viscous layer nor by the boundary condition with the basement. It is only in the unstable regime (marked by positive real part of Λ) that the influence of the substratum of finite thickness is appreciable. It is for that reason that an asymptotic solution for nonzero values of the stability exponent will be developed in the next section. This approach is different from the one of *Triantafyllidis and Leroy* [1994] who concentrated on the condition of neutral stability.

The dependence of the functions f_{ij} on the dimensionless thickness of the substratum ωH_b is depicted in Figures 2a and 2b for the case of a perfect bond and a frictionless contact with the basement, respectively. The influence of the substratum thickness on the functions f_{ij} decays exponentially with ωH_b. The functions f_{ij} have larger values for a perfect bond than for a frictionless slip for the same ωH_b. For dimensionless substratum thickness ωH_b larger than 3 or 4, depending on the boundary conditions, the functions f_{ij} are approximately equal to the Kronecker delta function δ_{ij} (equal to 1 if i and j are identical and to 0 otherwise). This limiting value coincides with the result obtained by *Triantafyllidis and Leroy* [1994] for a half-space substratum.

The existence of a thickness threshold above which the susbstratum is equivalent to a half-space, which we estimate to be at most $4/\omega$ and denote H_c, has implications for the classification of instabilities in multilayered systems. A competent layer in a periodic system (consisting of competent and viscous layers) will buckle independently of its neighboring layers if the distance separating each layer is at least H_c. Conversely, the layers will interact if the separation distance is less than H_c. *Ramberg* [1960, 1961] follows an heuristic argument and then a more rigorous approach similar to ours to estimate the critical depth to be first $4/\omega$ and then $2\pi/\omega$. These estimates appear to coincide with measurements in the laboratory and in the field [*Ramberg,* 1960] and are similar to our value of $4/\omega$. The influence of the substratum and the value of H_c will be explored further in the fourth section.

The variational formulation (17) is valid for a large class of elastoplastic constitutive models. It is the basis for the development of the asymptotic solution, for a small overburden thickness compared to the instability wavelength, considered in the next section. It is also the starting point for the analytical solution obtained in ab-

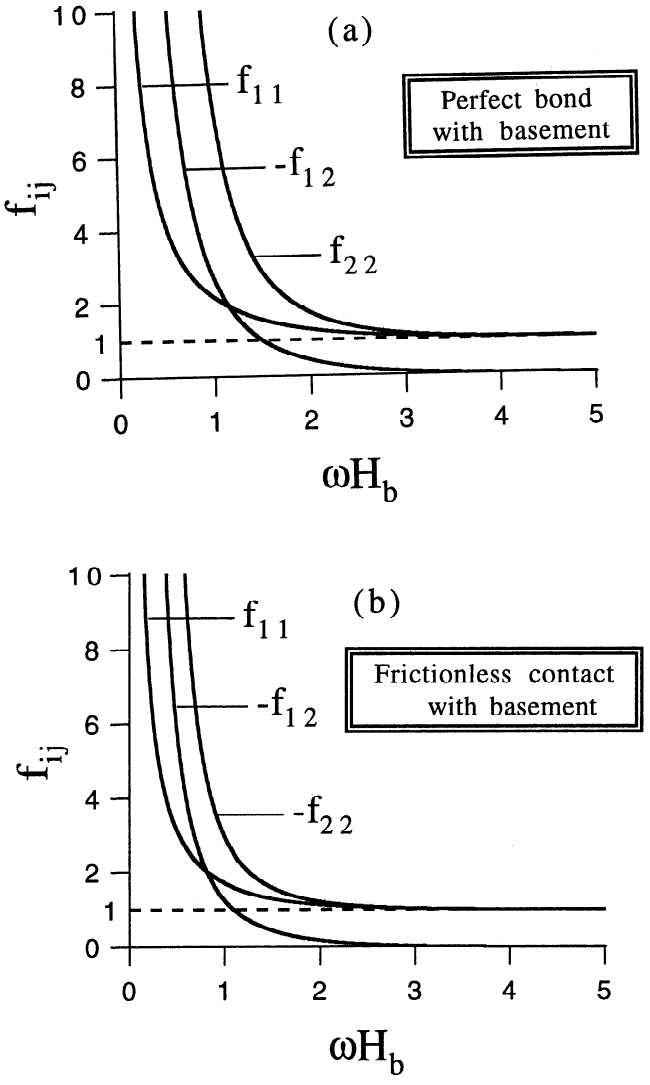

Figure 2. The influence of the substratum on the stability of the system is introduced by the functions f_{ij} of the dimensionless wavenumber ωH_b (H_b is the substratum thickness). Two boundary conditions are considered at the interface with the rigid basement: (a) no displacement (perfect bond) and (b) no vertical displacement and zero tangential traction (frictionless contact).

sence of gravity and for the approximate solution based on the finite element method which will be presented in the sequel to this work.

Stability Analysis

The presence of a stress gradient renders impossible the derivation of an analytical solution to the eigenvalue problem stated in (17) because of the spatial dependence of the nonlinear material coefficients. Nevertheless, an asymptotic solution can be obtained, for an overburden thickness small compared to the perturbation wavelength ($\omega H_a \ll 1$) and is presented in the second part of this section. Before presenting the asymptotic analysis, it is instructive to comment on some classical results concerning the stability of an axially prestressed elastic plate resting on a viscous foundation. These results, based on strength of materials analyses [e.g., *Timoshenko*, 1936], are helpful in explaining the origins of our asymptotic analysis and in providing the structure of the results discussed in the next section.

Case of an Elastic Plate

The equation governing the stability of an infinitely long elastic plate sustaining a uniform compressive axial stress σ_0, under plane strain conditions, and which rests on a linear viscoelastic medium of infinite extent reads

$$\frac{\Lambda}{G} = -\frac{\overset{b}{\rho}\, g}{\omega G} - (\omega H_a)\frac{\sigma_0}{G} - (\omega H_a)^3 \frac{1}{6(1-\nu)}, \qquad (20)$$

in which $\Lambda/G, G$ and ν are the dimensionless stability exponent of the system (Λ is positive if the system is unstable), the elasticity modulus in shear and Poisson's ratio, respectively. The stress σ_0 acting on the plate defined in (20) corresponds to the horizontal stress proposed in (1) if the angle φ and the gradients k_1 and k_3 are set to zero. The plate has thickness H_a and is perturbed with a wavelength $2\pi/\omega$. If neutral stability is of interest ($\Lambda = 0$), then (20) gives the condition for onset of buckling given by *Smoluchowski* [1909] and discussed by *Ramberg and Stephansson* [1964].

Equation (20) shows an explicit dependence of the stability exponent on the geometrical and material parameters of the model. An inspection of the sign of the three terms on the right-hand side of (20) reveals the stabilizing effect of gravity, the destabilizing influence of the tectonic compressive force (recall that a compressive stress is negative) and the stabilizing influence of the stiffness of the plate. An interpretation of (20) as a truncated asymptotic development for the small parameter ωH_a indicates that gravity, tectonic force and plate stiffness are found at the zero, first and third order of the development. To illustrate the competing influences of the tectonic force and the stiffness of the plate, several isocontours in Λ/G (solid curves) are plotted in Figure 3a in a space spanned by the dimensionless stress σ_0/G and wavenumber ωH_a. The shape of the neutral stability curve shows that for a given stress (take, for example, $(\sigma_0/G)_m$) the system is stable to small values of ωH_a (less than 0.014), unstable for an intermediate range and stable for large values of ωH_a. That structure is due to the stabilizing role of gravity and plate stiffness for small and large values of the wavenumber, respectively. The shape of any isocontour of Λ_1 is similar to the one described for neutral stability. Consequently, for a given stability exponent Λ/G (positive if unstable) and a given stress σ_0/G, there are zero, one or two admissible values of the wavenumber ωH_a. Furthermore, there exists a minimum stress $(\sigma_0/G)_m$ and an associated wavenumber $(\omega H_a)_m$ to trigger an instability at a given rate. These minimum values correspond to the point on the isocontour with a tangent parallel to the (ωH_a) axis, as illustrated in Figure 3a, and have the

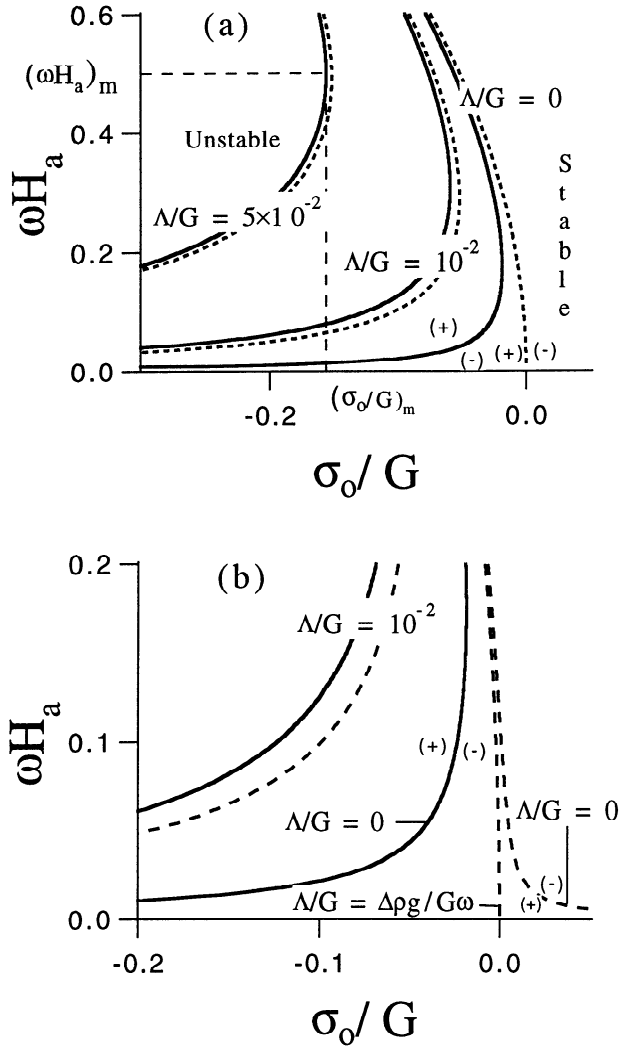

Figure 3. Stability diagram for an elastic plate on a viscous half-space in a space spanned by the dimensionless wavenumber ωH_a and stress σ_0/G. (a) Isocontours of dimensionless stability exponent Λ/G are depicted in the presence (solid curves) and in the absence (dotted curve) of gravity. (b) The former curves are compared with results obtained for the redistribution condition ($s = 1$) at the top surface (dashed curves). The plus and minus signs refer to the sign of the stability exponent and thus mark the unstable and stable regions, respectively.

following expressions extracted from (20)

$$(\sigma_0/G)_m = -\frac{3}{2}\left[\left(\frac{\overset{b}{\rho}\, g}{\omega G} + \frac{\Lambda}{G}\right)^2 \left(3(1-\nu)\right)^{-1}\right]^{1/3},$$
$$(\omega H_a)_m = \left[-(\sigma_0/G)_m 2(1-\nu)\right]^{1/2}. \qquad (21)$$

Note from (21) that the influence of the substratum viscosity is only felt through the stability exponent (recall that Λ is defined as $2\lambda\, \overset{b}{\mu}$). Furthermore, the relation between $(\sigma_0/G)_m$ and $(\omega H_a)_m$ is independent of the substratum density.

In Figure 3a, the stability exponent isocontours obtained disregarding gravity have also been drawn (dotted curves). By setting g to zero in (20) or by comparing the curves in Figure 3a obtained in the absence and the presence of gravity, one realizes that gravity is unimportant in the unstable regime if the stability exponent Λ/G is large compared to the dimensionless number $\overset{b}{\rho}\, g/\omega G$. However, the difference between the two types of curves is noticeable for small value of the stability exponent compared to the number $\overset{b}{\rho}\, g/\omega G$, especially for small values of ωH_a. Moreover, the singular behavior of the neutral stability isocontour in the presence of gravity for vanishing ωH_a, is replaced by a semiparabola going through the origin if gravity is not accounted for. There is thus a range of the stability exponent for which gravity does not play an essential role ($\overset{b}{\rho}\, g/\omega G \ll \Lambda/G$). This remark prompts the search for a solution to the stability problem in the absence of gravity. In that instance, there is no spatial dependence of the material coefficients entering (17) and the solution, presented in the sequel of this work, is analytical.

The plate model is easily extended to account for redistribution at the top free surface (8) by replacing the fluid of density $\overset{b}{\rho}$ with a fluid of density $\overset{b}{\rho} - \overset{a}{\rho}$

$$\frac{\Lambda}{G} = \frac{\Delta\rho g}{\omega G} - (\omega H_a)\frac{\sigma_0}{G} - (\omega H_a)^3 \frac{1}{6(1-\nu)}, \qquad (22)$$

in which $\Delta\rho$ is defined as the density contrast $\overset{a}{\rho} - \overset{b}{\rho}$. This modification to account for redistribution is consistent with the condition proposed by *Biot and Odé* [1965] and presented in (8). If the density contrast is negative, the stability exponent isocontours are similar to the ones described above. Of more interest is the case of a substratum lighter than the overburden ($\Delta\rho > 0$) for which the shape of the stability exponent isocontours differs. This is illustrated by three dashed curves in Figure 3b. The role of the sign of $\Delta\rho$ is clearly seen by replacing in (21) the density $\overset{b}{\rho}$ by $-\Delta\rho$. Then, the minimum dimensionless stress $(\sigma_0/G)_m$ exists only if the dimensionless stability exponent exceeds $\Delta\rho g/\omega G$ as it is the case for $\Lambda/G = 10^{-2}$ in Figure 3b. If these two quantities are equal, the isocontour is a semiparabola intersecting the origin of the graph, as it can be inferred from (22) and seen in Figure 3b. For a dimensionless stability exponent less than $\Delta\rho g/\omega G$, the shape of the isocontours is such that there is no minimum stress $(\sigma_0/G)_m$. For example, the isocontour for a stability exponent equal to zero enters the region of positive prestress (Figure 3b).

Asymptotic Analysis for a Thin Overburden

These simple results are now extended to the case of a time-independent, elastoplastic overburden with a complex in situ stress gradient and a substratum of finite thickness. From the structure of (20), it seems logical to search for an asymptotic development of the dimensionless stability exponent Λ/G in terms of the small

parameter ωH_a (denoted ϵ in what follows). The unknown coefficients of this development should be functions of the substratum dimensionless thickness ωH_b, the stress parameters ($\sigma_0/G, k_1, k_3$ and φ), the dimensionless number $\Delta\rho g/\omega G$ and of the overburden material properties. It is found that this asymptotic expansion contains singular terms, and hence it is preferable to express $\Delta\rho g/\omega G$, instead of Λ/G, as a function of the small parameter ϵ. The reader is referred to *Triantafyllidis and Leroy* [1994] for further discussion on the treatment of this singularity in the special case of neutral stability. The option of choosing $\Delta\rho g/\omega G$ is thus adopted and the following development assumed

$$\frac{\Delta\rho g}{\omega G} = \gamma_0 + \epsilon\gamma_1 + \epsilon^2\gamma_2 + \epsilon^3\gamma_3 + \mathcal{O}(\epsilon^4) \qquad (23)$$

in which the scalars γ_p, $(p = 0, 1, 2, \ldots)$ are the problem's main unknowns and the small parameter ϵ denotes ωH_a. By analogy to the elastic solution in (22), an asymptotic analysis up to the third order should be sufficient to obtain the influence of lowest order of the elastoplastic overburden stiffness. The components of the eigenvector U_i, the stresses σ_{ij}, and the incremental moduli L_{ijkl} in (17) are assumed to have developments similar to (23):

$$U_i = \overset{0}{U}_i + \epsilon \overset{1}{U}_i + \epsilon^2 \overset{2}{U}_i + \epsilon^3 \overset{3}{U}_i + \mathcal{O}(\epsilon^4), \qquad (24)$$

$$\sigma_{ij}(\xi) = \overset{0}{\sigma}_{ij} + \epsilon \overset{1}{\sigma}_{ij}(\xi) + \epsilon^2 \overset{2}{\sigma}_{ij}(\xi) + \epsilon^3 \overset{3}{\sigma}_{ij}(\xi) + \mathcal{O}(\epsilon^4), \qquad (25)$$

$$L_{ijkl}(\xi) = \overset{0}{L}_{ijkl} + \epsilon \overset{1}{L}_{ijkl}(\xi) + \epsilon^2 \overset{2}{L}_{ijkl}(\xi) + \epsilon^3 \overset{3}{L}_{ijkl}(\xi) + \mathcal{O}(\epsilon^4), \qquad (26)$$

while the uniqueness of the eigenmode U_i is ensured by the following normalization condition

$$\int_0^1 [\overset{0}{U}_1 U_1 + \overset{0}{U}_2 U_2] d\xi = 1. \qquad (27)$$

A special feature of this analysis is the presence of a second small parameter, namely, the dimensionless stability exponent Λ/G. The values of this second parameter can be small compared to 1, in view of our interest for the system near criticality ($\Lambda/G = 0$). It is a standard technique in asymptotic analysis of problems with two small parameters, such as in elastic plate and shell theories [*Destuynder,* 1980; *Kohn and Vogelius,*1984], to assume that they are related by a simple power law such as

$$\Lambda = \epsilon^p \Lambda_p, \quad p = 0, 1, 2, \ldots \qquad (28)$$

Note that such a procedure has never been considered for nonlinear eigenvalue analyses to our knowledge. The adoption of p equal to 1 was found to be optimum for this problem. Indeed, the choice of p greater than 1 necessitates the study of terms higher than $\mathcal{O}(\epsilon^4)$ to incorporate the effect of the overburden's stiffness. The scalar Λ_1 is referred to as the scaled stability exponent in what follows.

The preliminary steps of the asymptotic analysis being taken, it remains to insert the proposed development (23)-(26) into the variational formulation (17), to collect the terms of like order in ϵ, and to solve the resulting variational problems at every order p for the main unknown γ_{p+1} introduced in (23). The complete solution is presented in the appendix and the details of the derivation are postponed to a supplement to this paper. Although the general expressions for γ_p are cumbersome, the results for the special case of a linearly elastic overburden which rests on an infinite substrate are simpler and recorded here:

$$\gamma_0 = 0, \quad \gamma_1 = \left[\frac{\sigma_0}{G}\cos(\varphi) + \frac{\Lambda_1}{G}\right]\frac{\Delta\rho}{\overset{a}{\rho} - \overset{b}{\rho}},$$

$$\gamma_2 = 0, \quad \gamma_3 = \frac{1}{6(1-\nu)}\frac{\Delta\rho}{\overset{a}{\rho} - \overset{b}{\rho}} \qquad (29)$$

for sake of comparison with the elastic solution (22). Indeed, recalling the definition of Λ_1 from (28) and noting that the absence of a lateral stress implies σ_{33} to be 0 (and hence $\cos(\phi) = 1$), the above results are found to be in agreement with (22). Note that it is necessary to disregard stress quantities compared to elastic modulus to obtain this result.

Results

Material parameters are selected in the first part of this section. The presentation of the asymptotic solution for the special case of the flow theory version of the Rudnicki and Rice model constitutes the second part. It should be noted that the asymptotic solution requires that the scalar ωH_a be small compared to 1. The assessment of the range of validity of the results to be presented is considered in the sequel of this work.

Material Parameter Selection

The variational formulation presented earlier is valid for a general class of elastoplastic models. The selection of a particular model dictates the incremental moduli presented in (3). The Rudnicki-Rice model adopted for the overburden is a finite strain generalization of the rate-independent, pressure-sensitive, isotropic hardening model of *Drucker and Prager* [1952] and depends on a single internal variable, the accumulated equivalent plastic strain γ^p. That scalar is computed by integrating through the loading history the equivalent plastic strain rate which is defined as the square root of twice the second invariant of the plastic part of the rate of deformation tensor. An explicit definition of γ^p and expressions for the moduli are found in equations (21) and (22) of *Triantafyllidis and Leroy* [1994].

It is assumed that laboratory tests have provided us with the uniaxial response of the overburden material which is fitted, for example, by a piecewise power law. This relation is generalized to multiaxial stress states by relating, with the same power law, the normalized equivalent plastic strain (γ^p/γ_y) to the normalized equivalent stress $(\tau + \mu p)/\tau_y$ in which μ is the friction coefficient. This relation corresponds to equation 109

of *Triantafyllidis and Leroy* [1994] and is depicted in Figure 4. The equivalent shear stress τ and pressure p are the square root of half the second invariant of the deviatory part of the Kirchhoff stress and the third of the first invariant of the Kirchhoff stress, respectively [*Triantafyllidis and Leroy,* 1994, eqs. 23]. The scalar τ_y is the yield stress which can be related to the material cohesion while the yield strain γ_y is defined as τ_y/G. In Figure 4 we observe a linear relation between equivalent stress and strain for a strain less than γ_y. This relation becomes nonlinear once this deformation is exceeded. This is due to the work hardening governed by the power law exponent m (Figure 4a) but not by the yield strain (Figure 4b). The exponent m lies between 1 and $+\infty$ corresponding to the two limits of an elastic and of an elastic, perfectly plastic response, respectively. A value of 5 for m is chosen for all calculations unless otherwise stated.

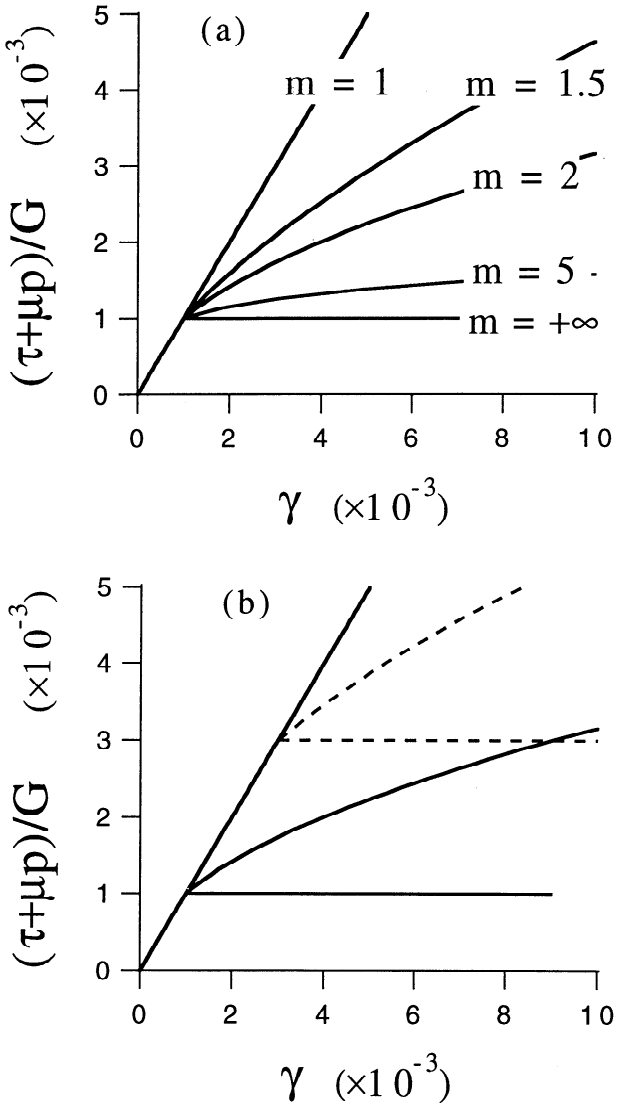

Figure 4. The uniaxial stress-strain curve for the overburden material. (a) The influence of the hardening exponent m is depicted for a yield strain of 0.001. (b) The dotted stress-strain curves corresponds to a yield strain of 0.003. The hardening exponent has for values 1, 2, or $+\infty$.

The elastic properties of the overburden are constant for all calculations, with an elastic modulus E of 10^{10} Pa and Poisson's ratio ν of 0.2. The friction coefficient μ is set to 0.6 while plastic dilatancy is disregarded. The yield stress τ_y is set to $\tau_y = 10^{-3}E$. These values are typical for sedimentary rocks (see *Mandl* [1988] for general references). The densities of the solid overburden and the viscous substratum are 2.5×10^3 kg/m^3 and 2.2×10^3 kg/m^3, respectively. These values are close to the ones chosen by *van Keken et al.* [1993] for their analysis of salt diapirism.

The perturbation considered has a wavenumber of 5×10^{-3}m^{-1} corresponding to a wavelength of, approximately, 1.26 km. The dimensionless number $\Delta\rho g/G\omega$ considered for the asymptotic development is thus fixed to 1.41×10^{-4}. The stress gradient k_1 and k_3 and the stress orientation angle φ are set to zero with the exception of a subsection.

Discussion of Results

The results are presented in four parts. In the first part (Figures 5 and 6) the influence on stability of the substratum thickness and the boundary conditions at the basement is investigated. The second part (Figures 7 and 8) pertains to a discussion on the role of the stress gradient parameter k_1 and the orientation angle φ. The influence of the work-hardening exponent m is examined in the third part. For all the calculations reported here, the condition (3) of strong ellipticity was checked but an onset of faulting was never detected. A short discussion of this finding constitutes the last part of this section.

In all the figures to be presented, the horizontal and vertical axes correspond to the dimensionless stress parameter σ_0/τ_y and to the dimensionless wavenumber ωH_a, respectively. The range covered by ωH_a is from 0 to 2. The isocontours of the scaled stability exponent, Λ_1, are always plotted in the unstable domain delimited by the neutral stability curves. Unstable and stable domains are marked by a minus and a plus sign. They correspond to the sign of the stability exponent. A point with coordinates $(\sigma_0/\tau_y)_{\Lambda_1}$ and $(\omega H_a)_{\Lambda_1}$ on an isocontour Λ_1 provides the thickness of the unstable overburden $(H_a)_{\Lambda_1} = (\omega H_a)_{\Lambda_1}/\omega$ which sustains a prestress characterized by $(\sigma_0/\tau_y)_{\Lambda_1}$ and for which a perturbation with wavenumber ω grows at an initial rate $(\Lambda_1 \omega H_a/2\overset{b}{\mu})$.

Influence of geometry. The influence of the substratum thickness on stability for a perfect bond at the basement is presented in Figures 5a (ωH_b is set to 3, 4, and $+\infty$) and 5b (ωH_b equal to 1). Four series of isocontours of scaled stability exponent are drawn in Figure 5a including the neutral stability case. For each series, the solid, dotted and dashed curves correspond to the three values of $+\infty$, 4, and 3 for ωH_b, respectively. These values were chosen to test the validity of the conclusion drawn earlier that the basement has no influence on the stability of the competent layer if the dimension-

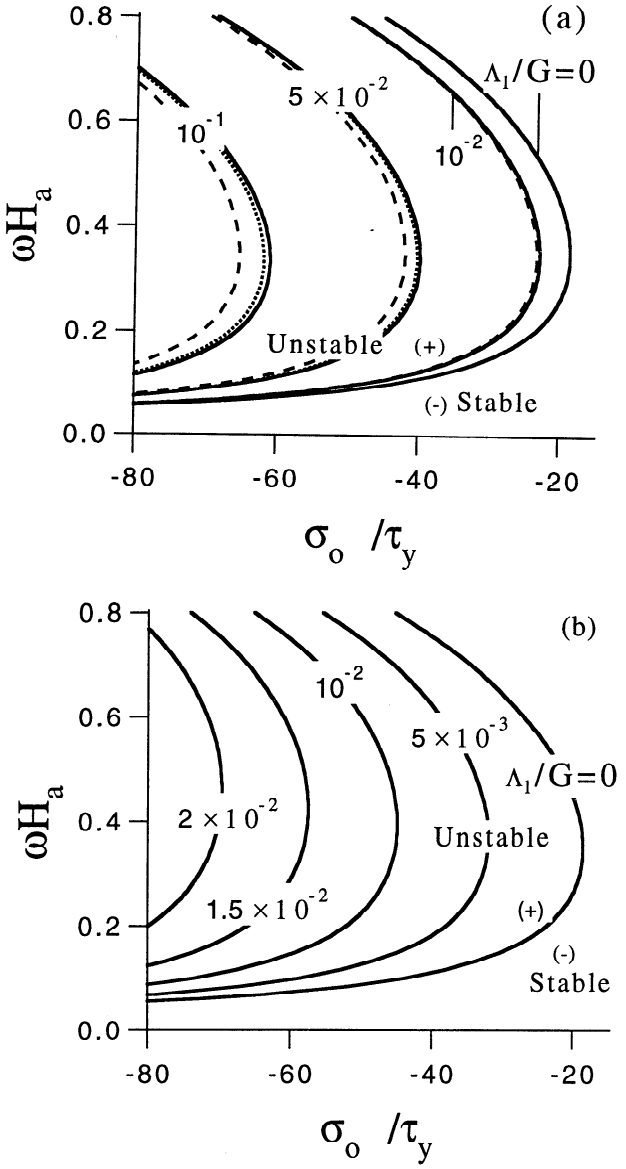

Figure 5. Influence on stability of the substratum thickness for the case of a perfect bond with the basement. The isocontours of dimensionless, scaled stability exponent Λ_1/G ($\Lambda_1 = \Lambda/\omega H_a$, with Λ proportional to the perturbation rate of growth if positive) are drawn in a space spanned by the dimensionless overburden thickness ωH_a and stress σ_0 normalized by the cohesion τ_y. (a) The solid, dotted, and dashed lines are obtained for a dimensionless substratum thickness ωH_b set to $+\infty$, 4, and 3, respectively. (b) Variable ωH_b is set to 1.

less substratum thickness ωH_b exceeds 4 (see Figure 2). The neutral stability curve in this figure, independent of ωH_b, shows that the account of the overburden cohesion guarantees the existence of a stable regime for compressive stresses below a certain magnitude. This is in contrast to the result of stability analyses based on viscoelastic models, but in agreement with the neutral stability results for an elastic plate (see Figure 3). Observe from Figure 5a that the influence of ωH_b on Λ_1/G is still felt for a value of 3 but that there is little difference between the isocontours obtained for ωH_b of either 4 or $+\infty$. Notice also that the distance between isocontours obtained for various ωH_b diminishes close to the neutral stability curve: the latter is independent of the value of the substratum thickness and of the boundary conditions at the basement.

The isocontours in Figure 5b, obtained for ωH_b set to 1, are drawn for five values of the dimensionless stability exponents Λ_1/G. These values differ from the ones considered in Figure 5a, with the exception of the neutral stability and for $\Lambda_1/G = 10^{-2}$. A comparison between the two isocontours $\Lambda_1/G = 10^{-2}$ in Figures 5a and 5b shows that the stress required to initiate an instability at that rate is multiplied approximately by a factor of 2 as the substratum thickness changes from 6 km ($\omega H_b = 3$) to 2 km ($\omega H_b = 1$). The thicker the substratum, the fastest is the instability growth for the same tectonic stress and pertubation wavelength. The neutral stability contours in these two figures are identical since they are unaffected by the thickness of the substratum.

The influence of the boundary conditions at the basement is evidenced by comparing Figures 5b and 6, the former drawn for a perfect bond and the latter for frictionless slip. To facilitate this comparison, the values of Λ_1/G considered in Figure 5b are also used in Figure 6. The four isocontours in the unstable regime of Figure 5b are shifted to the right in Figure 6, closer to the neutral stability curves. Hence, to initiate an instability for a given (ωH_a) at a given scaled stability exponent, a larger stress magnitude is required for perfect bonding than for frictionless sliding at the base-

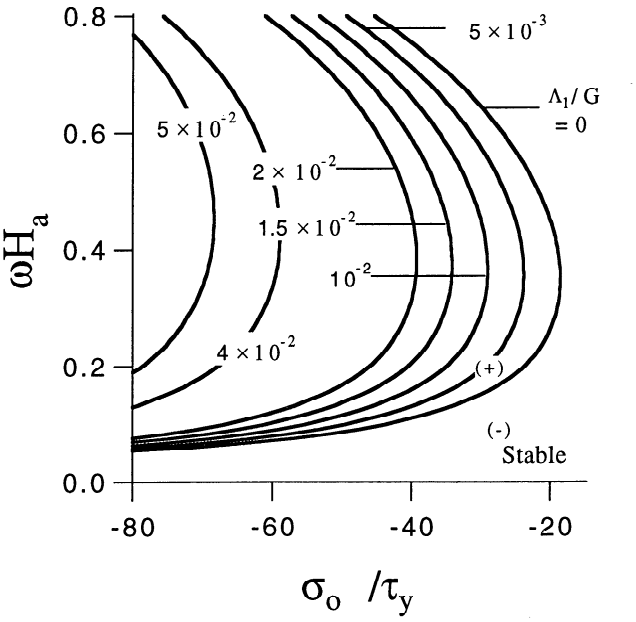

Figure 6. Influence on stability of the boundary condition between basement and substratum. The iscontours of scaled stability exponent, obtained for frictionless slip with the basement and a dimensionless substratum thickness ωH_b set to 1, should be compared to those presented in Figure 5b.

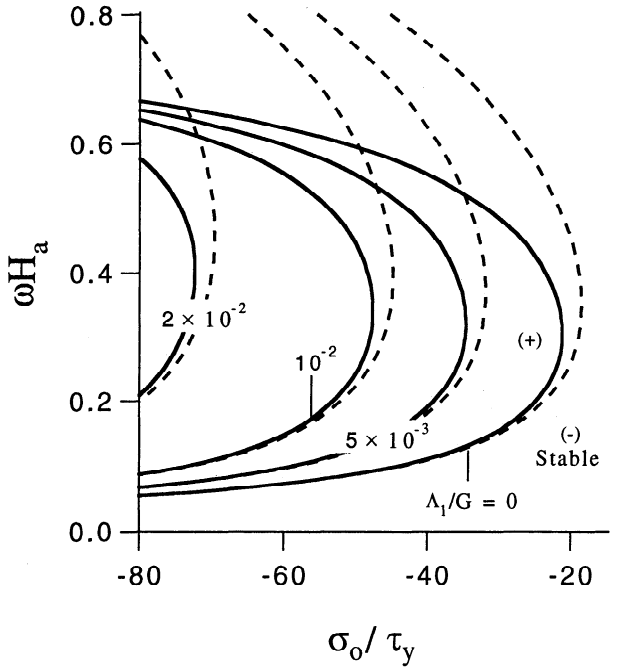

Figure 7. Influence on stability of the stress gradient k_1. The solid and dashed curves (isocontours of scaled stability exponent) correspond to k_1 equal to 2 and 0, respectively. Results obtained for a dimensionless substratum thickness ωH_b set to 1 and a perfect bond with the basement.

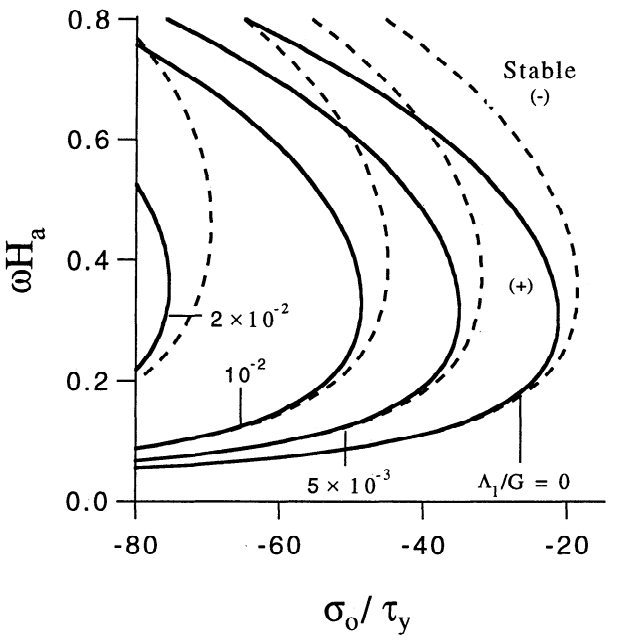

Figure 8. Influence on stability of the stress orientation angle φ. The solid and dashed curves (isocontours of scaled stability exponent) correspond to φ set to $\pi/2$ and 0, respectively. Results obtained for a dimensionless substratum thickness ωH_b set to 1 and a perfect bond with the basement.

ment contact. The ratio between these two magnitudes is close to 1.7 for an ωH_b equal to 1. The perfect bond is thus stabilizing compared to the frictionless slip condition. Concerning the influence of the substratum thickness for the frictionless sliding case, a figure similar to Figure 5a (not presented here for sake of conciseness) would show that the critical dimensionless thickness required for the influence of the basement not to be felt by the competent layer is 3. It differs from the value of 4 found for perfect bonding and confirms the destabilizing influence of frictionless sliding at the basement. These results are in agreement with the discussion of Figure 2 given earlier.

Stress gradient and orientation effects. The role of the stress gradient parameter k_1 and orientation angle φ, defined in (1) and in Figure 1b, is analyzed in Figures 7 and 8. The lateral stress gradient with depth is proportional to the lithostatic pressure gradient, with k_1 being the proportion constant. The classical plate solutions, discussed in the previous section, disregard the stress gradient ($k_1 = 0$) which is typically of order 1 in sedimentary basins [*Breckels and van Eekelen,* 1982] and of order 2 in certain folded regions [*McGarr and Gay,* 1978]. Concerning the angle φ, recall that the ratio of principal stresses along the x_1 and x_3 coordinate axes at the overburden-substratum interface is $\tan(\varphi)$. A uniaxial compression along the x_1 or x_3 axis corresponds to φ equal to zero or $\pi/2$, respectively.

The influence of these two parameters k_1 and φ (Figures 7 and 8) appears to be minor for small values of ωH_a (in the range $\omega H_a < 0.2$). However, for larger values of the dimensionless overburden thickness, the shape of the iscocontours depends strongly on k_1 and φ: the range of overburden thicknesses which can be destabilized for a given σ_0 decreases with increasing values of k_1 and decreasing values of φ. This influence appears in a range of ωH_a for which the validity of the asymptotic results is an open question and we shall thus postpone to a future paper (which deals with the validation of the asymptotic solution) the confirmation of these results.

Influence of work hardening. The influence of the work hardening exponent m is shown in Figure 9. A power law hardening function has been chosen such that the values of m equals to 1 and $+\infty$ correspond to a linear elastic and an elastic, perfectly plastic response, respectively (see Figure 4). It is surprising to see that a large change in m from 1.5 to 5 has so little effect on the stability results (Figure 9). Note that the difference between two isocontours obtained for the same Λ_1/G but different m is approximately independent of the value of the scaled stability exponent. The results obtained with m equal to 10, not presented here, did not show any appreciable deviations from the isocontours obtained for an m of 5. These remarks indicate that the instability is dominated by geometric effects and not by the precise nature of the work-hardening law adopted for the overburden. An inspection of the slenderness of the competent layer for a typical ωH_a of 0.5 shows a length-to-thickness aspect ratio of the order of 100, confirming this interpretation. The influence of

work hardening can be more pronounced for smaller aspect ratios and will be explored in the sequel of this work.

Investigation of faulting. For all the calculations reported above, the condition of strong ellipticity, the violation of which signals the onset of faulting, was checked. The initiation of faulting was never detected, even for the low hardening case with an exponent m of 10. The absence of faulting in the unstable regime, despite the weak work hardening employed, forces us to question the appropriateness of the flow theory version of the Rudnicki and Rice model for this problem. Indeed, it seems rather unrealistic that a stress magnitude 4 times larger than the one required to initiate folding is not sufficient to trigger faulting. The sensitivity of the ellipticity condition to the details of the plasticity model was discussed extensively by *Rudnicki and Rice* [1975]. They show that a deformation theory of plasticity, which accounts in a simple way for the presence of small faults or cracks to accommodate the deformation, was more conducive to faulting than the corresponding flow theory. *Triantafyllidis and Leroy* [1994] used the deformation theory of the Rudnicki and Rice model and found a strong influence on their structural stability results. We shall use such a deformation theory in the second part of this work to study its influence on the stability of this stratified system.

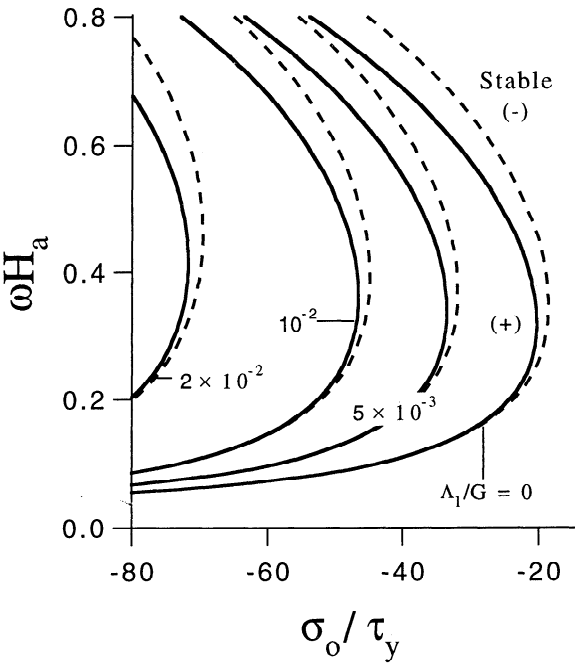

Figure 9. Influence on stability of the hardening exponent m. The solid and dashed curves (isocontours of scaled stability exponent) corresponds to an exponent m of 1.5 and 5, respectively. Results obtained for a dimensionless substratum thickness ωH_b set to 1 and a perfect bond with the basement.

Conclusion

A variational formulation has been established to model the stability of a stratified system composed of a time-independent elastoplastic overburden overlying a viscous substratum resting on a rigid basement. It is shown that the system is equivalent to a competent layer over a substratum of infinite thickness if the product of the perturbation wavenumber and the substratum thickness is larger than 3 for a frictionless contact or 4 for a perfect bond with the basement. The substratum thickness and boundary conditions do not influence neutral stability.

An asymptotic solution to the system's variational formulation has been presented which extends the classical solution for stability of an elastic plate resting on a fluid in three ways: the plate is elastoplastic, the stress distribution is not uniform but has a gradient with depth, and the viscous substratum has a finite thickness. This method, valid for a general class of plasticity models, and applied here to the flow theory version of the Rudnicki and Rice model, provides the height of an unstable overburden for a given stability exponent and stress state. Stability is not solely governed by density contrast, as in the case for viscoelastic systems, but is influenced by tectonic force. Stability is ensured for small magnitudes of the in situ compressive stress. For larger stress magnitudes, the in situ stress gradient and the stress orientation angle influence the range of overburden thicknesses for which the system is unstable. The rate of growth of the instability is found to be larger for thicker substratum. A condition of frictionless slip with the basement has a destabilizing influence compared to a perfect bond. Since geometric effects dominate in this problem, the role of the work hardening in the plasticity model appears to be minor. However, the absence of an onset of faulting for relatively large stresses suggests that the classical flow theory of plasticity may not be appropriate to model local modes of instability such as faulting.

In the sequel of this paper it will be shown that the stresses required to initiate faulting and folding modes of instability are of comparable magnitudes, if a deformation theory of plasticity is adopted. Deformation theories of plasticity account in a simple way for the destabilizing influence of a deformation mechanism by slip along cracks and small faults [*Rudnicki and Rice,* 1975]. A plasticity model built from the description of such a micro mechanism is proposed by *Leroy and Sassi* [1996] to study fractured formations. In the sequel, an analytical solution of the linear stability problem in the absence of gravity and a finite element approximation, which is used to assess the validity of the asymptotic solution, are also presented. Furthermore, these linear stability analyses are applied to a prototype, of the same geometry as the model considered here, for a section revealed by a seismic dipline through the Campos basin, offshore Brazil [*Demercian et al.,* 1993]. The two stages of folding that occurred during the Albian and the tertiary are then analyzed. Similar stability analyses are also applied to a scaled prototype of the same field case for laboratory experiments to show the diffi-

culty in producing adequately both folding and faulting with conventional analogue materials.

A linear stability analysis constitutes the first step of a complete nonlinear structural analysis. Those nonlinear calculations are based, in general, on a numerical approximation which can be tested by comparing the numerical solution for the initial evolution in time of a perturbation with the solution of the linearized problem. Such a comparison was considered by *Massin et al.* [1996] who use the finite element method to study the formation of folds of finite amplitude and of chevron type of structures starting from a geometry identical to the one considered here. These stability predictions could also contribute to the numerical analyses of a variety of geological problems. It suffices here to mention the initiation of rift structures [*Ricke and Mechie,* 1989] and the relevance of layer-parallel slip for understanding the spatial variation of in situ stress in sedimentary basins [*Sassi and Faure,* 1996].

Appendix: Asymptotic Solution

The asymptotic solution for small overburden thickness ($\epsilon \equiv \omega H_a \ll 1$), which was presented in the main text for the elastic case, is now presented for an elastoplastic overburden. The details of the derivation are postponed to the supplement of this paper.

The coefficient γ_0 and γ_1 entering the development in (23) takes the form

$$\gamma_0 = 0\,, \tag{A1}$$

$$\gamma_1 = \Big[\sigma_0 \cos(\varphi) + \Lambda_1 \big[f_{22} - \frac{f_{12} f_{21}}{f_{11} + (\overset{0}{E_t}/\Lambda_1)}\big]\Big] \frac{\Delta\rho}{(s\overset{a}{\rho} - \overset{b}{\rho})G}\,. \tag{A2}$$

Any coefficient γ_α, with α larger or equal to 2, admits the general representation

$$\gamma_\alpha = \frac{\overset{\alpha}{h_i}\overset{0}{U_i}}{\overset{0}{U_2}\overset{0}{U_2}} \frac{\Delta\rho}{(s\overset{a}{\rho} - \overset{b}{\rho})G}\,, \tag{A3}$$

in which the zero-order eigenvector components $\overset{0}{U_i}$ are defined by

$$\overset{0}{U_1} = -\overset{0}{U_2}\frac{f_{12}}{f_{11} + (\overset{0}{E_t}/\Lambda_1)}\,,$$

$$\overset{0}{U_2} = \left[1 + \left[\frac{f_{12}}{f_{11} + (\overset{0}{E_t}/\Lambda_1)}\right]^2\right]^{-1/2}\,. \tag{A4}$$

The components $\overset{\alpha}{h_i}$ introduced in (A3) have for expression

$$\overset{2}{h_1} = \Big[-\frac{\overset{0}{E_t}}{2} + \frac{\overset{0}{L_{1122}}}{\overset{0}{L_{2222}}}\Big(\frac{\sigma_0\cos(\varphi)}{2} - s\frac{\overset{a}{\rho}G}{\Delta\rho}\gamma_1\Big) + \frac{\overset{a}{\rho}G}{\Delta\rho}\gamma_1\Big]\overset{0}{U_2}\,,$$

$$\overset{2}{h_2} = \Big[-\frac{\overset{0}{E_t}}{2} + \frac{\overset{0}{L_{2211}}}{\overset{0}{L_{2222}}}\Big(\frac{\sigma_0\cos(\varphi)}{2} - s\frac{\overset{a}{\rho}G}{\Delta\rho}\gamma_1\Big) + \frac{\overset{a}{\rho}G}{\Delta\rho}\gamma_1\Big]\overset{0}{U_1}\,, \tag{A5}$$

for the second order and

$$\overset{3}{h_1} = \int_0^1 \Big[\overset{0}{E_t}\int_0^\xi \frac{d\overset{2}{U_1}}{d\xi}d\xi - \frac{\overset{0}{L_{1122}}}{\overset{0}{L_{2222}}}\varphi_2(\xi) + (\overset{2}{L_{1111}}(\xi) - \overset{2}{L_{1122}}(\xi)\frac{\overset{0}{L_{2211}}}{\overset{0}{L_{2222}}})\overset{0}{U_1}\Big]d\xi + \frac{\overset{a}{\rho}G}{\Delta\rho}(\gamma_1\overset{1}{U_2}(0) + \gamma_2\overset{0}{U_2})\,,$$

$$\overset{3}{h_2} = \int_0^1 \Big[\sigma_0\cos(\varphi)\int_0^\xi \frac{d\overset{2}{U_2}}{d\xi}d\xi + \varphi_1(\xi) + \overset{2}{\sigma}_{11}(\xi)\overset{0}{U_2} - s\frac{\overset{a}{\rho}G}{\Delta\rho}\Big(\gamma_1\frac{d\overset{2}{U_2}}{d\xi} + \gamma_2\frac{d\overset{1}{U_2}}{d\xi}\Big)\Big]d\xi - s\frac{\overset{a}{\rho}G}{\Delta\rho}\gamma_2\overset{1}{U_2}(0) + \frac{\overset{a}{\rho}G}{\Delta\rho}(\gamma_1\overset{1}{U_1}(0) + \gamma_2\overset{0}{U_1}) + \frac{\overset{b}{\rho}G}{\Delta\rho}\gamma_2\overset{1}{U_2}(0)\,, \tag{A6}$$

for the third order. Note that the asymptotic analysis can be stopped at the third order. Indeed, we know, from the simplified analysis presented for a compressed beam in a viscous medium of infinite extent, that the third-order term γ_3 is the term of lowest order which contains a contribution of the stiffness of the overburden. Accuracy of the asymptotic development would be the only reason to continue the calculations further. In the last set of two equations (A6), the two functions $\varphi_i(\xi)$ are defined by

$$\varphi_1(\xi) = \frac{\overset{a}{\rho}G}{\Delta\rho}\gamma_1(\xi-1)\overset{0}{U_2} + \overset{0}{E_t}\Big[(\xi-1)\overset{1}{U_1}(0) - \frac{1}{2}(\xi^2-1)\overset{0}{U_2}\Big] - \frac{\overset{0}{L_{1122}}}{\overset{0}{L_{2222}}}\Big[\sigma_0\cos(\varphi)\Big(\frac{1}{2}\xi^2 - \xi + \frac{1}{2}\Big) + s\frac{\overset{a}{\rho}G}{\Delta\rho}\gamma_1(\xi-1)\Big]\overset{0}{U_2}\,;$$

$$\varphi_2(\xi) = (\overset{2}{L_{2211}}(\xi) - \overset{2}{L_{2222}}(\xi)\frac{\overset{0}{L_{2211}}}{\overset{0}{L_{2222}}})\overset{0}{U_1} + s\frac{\overset{a}{\rho}G}{\Delta\rho}\Big[\gamma_1\Big(\overset{1}{U_2}(0) + \frac{\overset{0}{L_{2211}}}{\overset{0}{L_{2222}}}\overset{0}{U_1}\Big) + \gamma_2\overset{0}{U_2}\Big] + \overset{0}{E_t}\Big(\frac{1}{2}\xi^2 - \xi + \frac{1}{2}\Big)\overset{0}{U_1} + \sigma_0\cos(\varphi)\Big[(\xi-1)\overset{1}{U_2}(0) + \frac{\overset{0}{L_{2211}}}{\overset{0}{L_{2222}}}\frac{1}{2}(\xi^2-1)\overset{0}{U_1}\Big]\,. \tag{A7}$$

Equations (A6) and (A7) require the provision of the components of the first-order eigenvector

$$\overset{1}{U}_i(\xi) = \overset{1}{\alpha}\overset{0}{U}_i + \overset{1}{V}_i + \int_0^{\xi} \frac{d\overset{1}{U}_i}{d\xi} d\xi ,$$

$$\overset{1}{\alpha} = \frac{1}{2}\overset{0}{U}_1\overset{0}{U}_2\left[1 - \frac{\overset{0}{L}_{2211}}{\overset{0}{L}_{2222}}\right],$$

$$\overset{1}{V}_1 = \frac{-\overset{2}{h}_1(\overset{0}{E}_t + \Lambda_1 f_{11})}{(\overset{0}{E}_t + \Lambda_1 f_{11})^2 + (\Lambda_1 f_{12})^2},$$

$$\overset{1}{V}_2 = \frac{-\overset{2}{h}_1 \Lambda_1 f_{12}}{(\overset{0}{E}_t + \Lambda_1 f_{11})^2 + (\Lambda_1 f_{12})^2}, \qquad \text{(A8)}$$

which, in turn, are defined in terms of the following gradients

$$\frac{d\overset{1}{U}_1}{d\xi} = -\overset{0}{U}_2 , \quad \frac{d\overset{1}{U}_2}{d\xi} = \frac{\overset{0}{L}_{2211}}{\overset{0}{L}_{2222}}\overset{0}{U}_1 . \qquad \text{(A9)}$$

Note that the computation of $\overset{3}{h}_i$ in (A6) requires also the gradient of the second-order eigenvector which is found to be

$$\frac{d\overset{2}{U}_1}{d\xi} = \frac{\overset{0}{E}_t(\xi - 1)}{\overset{0}{L}_{1221}}\overset{0}{U}_1 - \overset{1}{U}_2(\xi) ,$$

$$\frac{d\overset{2}{U}_2}{d\xi} = \frac{\sigma_0 \cos(\varphi)(\xi - 1) + s\dfrac{\overset{a}{\rho} G}{\Delta\rho}\gamma_1}{\overset{0}{L}_{2222}}\overset{0}{U}_2 + \frac{\overset{0}{L}_{2211}}{\overset{0}{L}_{2222}}\overset{1}{U}_1(\xi) . \qquad \text{(A10)}$$

In these equations, the notation E_t has been reserved for the tangent moduli, classical in plate theories, which has for expression $E_t \equiv L_{1111} - L_{1122}L_{2211}/L_{2222}$.

Acknowledgments. Part of this work was conducted while the first author was affiliated with Shell Research, KSEPL. Permission to publish was granted by Shell Internationale Research Maatschappij B. V. Helpful discussions with J. L. Urai and the continuous encouragement of F. K. Lehner, both at KSEPL, are gratefully acknowledged. This paper is dedicated to G. Mandl, Technical University of Graz, on his 70th birthday. G. Mandl has promoted the use of plasticity theories to study faulting in the tectonic stress field. We hope this paper will contribute to the continuation of his work toward an integrated approach to analyze the initiation of faulting and folding.

References

Biot, M.A., Theory of folding of stratified visco-elastic media and its implication in tectonics and orogenesis, *Geol. Soc. Am. Bull., 72*, 1595-1620, 1961.

Biot, M.A., *Mechanics of Incremental Deformation*, John Wiley, New York, 1965.

Biot, M.A., and H. Odé, Theory of gravity instability with variable overburden and compaction, *Geophysics, 30*, 213-227, 1965.

Biot, M.A., H. Odé, and W.L. Roever, Experimental verification of the theory of folding of stratified viscoelastic media, *Geol. Soc. Am. Bull., 72*, 1621-1632, 1961.

Bishop, R.S., Mechanism for emplacement of piercement diapirs, *AAPG Bull., 62*, 1561-1583, 1978.

Breckels, I.M., and H.A.M. van Eekelen, Relationship between horizontal stress and depth in sedimentary basins, *J. Pet. Technol., 9*, 2191-2199, 1982.

Chapple, W.N., Fold shape and rheology: The folding of an isolated viscous-plastic layer, *Tectonophysics, 7*, 97-116, 1969.

Charo, L., and P. Habib, Potential for creation of a salt dome following disposal of radioactive waste in a salt layer (in French), vol. 1, Comm. des Communautés eur., Luxembourg, *11081*, 1987.

Coelewij, P.A.J., G.M.W. Haug, and H. van Kuijk, Magnesium-salt exploration in the northeastern Netherlands, *Geol. Mijnbouw, 57*, 487-502, 1978.

Demercian, S., P. Szatmari, and P.R. Cobbold, Style and pattern of salt diapirs due to thin-skinned gravitational gliding, Campos and Santos basins, offshore Brazil, *Tectonophysics, 228*, 393-433, 1993.

Destuynder, P., Sur une justification des modèles de plaques et coques par les méthodes asymptotiques, thèse de doctorat d'Etat, Univ. of Paris VI, 1980.

Dorris, J.F., and S. Nemat Nasser, Instability of a layer on a half space, *J. Appl. Mech., 47*, 304-312, 1980.

Drucker, D.C., and W. Prager, Soil mechanics and plastic analysis or limit design, *Q. J. Mech. Appl. Math., 10*, 157-165, 1952.

Fletcher, R.C., Wavelength selection in the folding of a single layer with power-law rheology, *Am. J. Sci., 274*, 1029-1043, 1974.

Fletcher, R.C., and B. Hallet, Unstable extension of the lithosphere: A mechanical model for basin-and-range structure, *J. Geophys. Res., 88*, 7457-7466, 1983.

Griggs, D., and J. Handin, Observations on fracture and a hypothesis of earthquake, in *Rock Deformation*, edited by D. Griggs and J. Handin, *Mem. Geol. Soc. Am., 79*, 347-373, 1960.

Hallbauer, D.K., H. Wagner, and N.G.W. Cook, Some observations concerning the microscopic and mechanical behaviour of quartzite specimens in stiff, triaxial compression tests, *Int. J. Rock Mech. Min. Sci. Geomech. Abstr., 10*, 713-726, 1973.

Hill, R., A general theory of uniqueness and stability in elastic-plastic solids, *J. Mech. Phys. Solids, 6*, 236-249, 1958.

Hill, R., and J.W. Hutchinson, Bifurcation phenomena in the plane tension test, *J. Mech. Phys. Solids, 23*, 239-264, 1975.

Kohn, R.V., and M. Vogelius, A new model for thin plates with rapidly varying thickness, *Int. J. Solids Struct., 20*, 333-350, 1984.

Leroy, Y.M., and W. Sassi, A plasticity model for discontinua, in *Aspects of Tectonic Faulting, Lecture Notes in Earth Sciences*, edited by F.K. Lehner, G. Riedmueller and E. Wallbrecher, Springer-Verlag, New York, in press, 1996.

Mandl, G., *Mechanics of Tectonic Faulting*, Elsevier, New York, 1988.

Martin, J.B., *Plasticity: Fundamentals and General Results*, MIT Press, Cambridge, Mass., 1975.

Martinod, J., and P. Davy, Periodic instabilities during compression or extension of the lithosphere, 1, Deformation modes from an analytical perturbation method, *J. Geophys. Res., 97*, 1999-2014, 1992.

Massin, P., N. Triantafyllidis, and Y.M. Leroy, Stability of density-stratified two-layer system, *C. R. Acad. Sci., Sér. IIa, Tectonique, 322*, 407-413, 1996.

McAdoo, D.C. and D.T. Sandwell, Folding of the oceanic lithosphere, *J. Geophys. Res., 90*, 8563-8569, 1985.

McGarr, A., and N.C. Gay, State of stress in the Earth's crust, *Annu. Rev. Earth Planet. Sci., 6*, 405-436, 1978.

Nettleton, L.L., and A. Elkins, Geologic models made from granular materials, *Eos Trans. AGU, 28*, 451-466, 1947.

Odé, H., Faulting as a velocity discontinuity in plastic deformation, in *Rock Deformation*, edited by D. Griggs and J. Handin, *Mem. Geol. Soc. Am., 79*, 293-321, 1960.

Ogden, R.W., *Non-Linear Elastic Deformations*, Ellis Horwood, Chichester, England, 1984.

Parker, T.J., and A.N. McDowell, Model studies of salt-dome tectonics, *Am. Assoc. Pet. Geol. Bull., 39*, 2384-2470, 1955.

Poirier, J.P., Shear localization and shear instability in materials in the ductile field, *J. Struct. Geol., 2*, 135-142, 1980.

Ramberg, H.R., Relationship between length of arc and thickness of ptygmatically folded veins, *Am. J. Sci., 258*, 36-46, 1960.

Ramberg, H.R., Contact strain and folding instability of multilayered body under compression, *Geol. Rundsch., 51*, 405-439, 1961.

Ramberg, H.R., and O. Stephansson, Compression of floating elastic and viscous plates affected by gravity, a basis for discussing crustal buckling, *Tectonophysics, 1*, 101-120, 1964.

Rice, J.R., The localization of plastic deformation, in *Theoretical and Applied Mechanics, Proc. of the 14th IUTAM Conference*, edited by W.T. Koiter, pp. 207–220, North-Holland, New York, 1976.

Ricke, M., and J. Mechie, Finite element modelling of a continental rift structure (Rhinegraben) with a large-deformation algorithm, *Tectonophysics, 165*, 81-91, 1989.

Rudnicki, J.W., and J.R. Rice, Conditions for the localization of the deformation in pressure-sensitive dilatant materials, *J. Mech. Phys. Solids, 23*, 371-394, 1975.

Sassi, W., and J.L. Faure, Role of faults and layer interfaces on the spatial variation of stress regime in basins: Inference from numerical modelling, *Tectonophysics*, in press, 1996.

Shemenda, A.I., Horizontal lithosphere compression and subduction: Constraints provided by physical modeling, *J. Geophys. Res., 97*, 11,097-11,116, 1992.

Sherwin, J.A., and W.N. Chapple, Wavelengths of single layer folds: A comparison between theory and observation, *Am. J. Sci., 266*, 167-179, 1968.

Smith, R.B., Unified theory of the onset of folding, boudinage, and mullion structure, *Geol. Soc. of Am. Bull., 86*, 1601-1609, 1975.

Smoluchowski, M., Über ein gerrisses Stabilitätsproblem der Elastizitätslehre und dessen Beziehung zur Entsehung von Faltengebirgen, *Abh. Akad. Wiss Krakau, Math. Kl.*, 3-20, 1909.

Tatsuoka, F., M.S.A. Siddiquee, C.S. Park, M. Sakamoto, and F. Abe, Modelling stress-strain relations in sand, *Soils Found., 33*, 60-81, 1993.

Timoshenko, S., *Theory of Elastic Stability*, McGraw-Hill, New York, 1936.

Triantafyllidis, N., and F. K. Lehner, Interfacial instability of density-stratified two-layer systems under initial stress, *J. Mech. Phys. Solids, 41*, 117-142, 1993.

Triantafyllidis, N., and Y.M. Leroy, Stability of a frictional material layer resting on a viscous half-space, *J. Mech. Phys. Solids, 42*, 51-110, 1994.

van Keken, P.E, C.J. Spiers, A.P van den Berg, and E.J. Muyzert, The effective viscosity of rocksalt: Implementation of steady-state creep laws in numerical models of salt diapirism, *Tectonophysics, 225*, 457-476, 1993.

van Wees, J.D., and S. Cloetingh, A finite-difference technique to incorporate spatial variations in rigidity and planar faults into 3-D models of the lithospheric flexure, *Geophys. J. Int., 117*, 179-195, 1994.

Wallace, M.H., and H.J. Melosh, Buckling of a pervasively faulted lithosphere, *Pure Appl. Geophys., 142*, 239-261, 1994.

Y. M. Leroy, Laboratoire de Mécanique des Solides, CNRS, URA 317, Ecole Polytechnique, Palaiseau 91128 Cedex, France. (email:leroyy@athena.polytechnique.fr)

N. Triantafyllidis, Department of Aerospace Engineering, University of Michigan, Ann Arbor, MI 48109-2140. (email:nick@engin.umich.edu)

(Received April 5, 1995; revised April 25, 1996;
accepted April 29, 1996.)